

# Study of cobalt-doped lithium–nickel oxides as cathodes for MCFC

Prabhu Ganesan, Hector Colon, Bala Haran, Ralph White, Branko N. Popov\*

Department of Chemical Engineering, Center for Electrochemical Engineering, University of South Carolina, Columbia, SC 29208, USA

Received 23 April 2002; accepted 8 May 2002

## Abstract

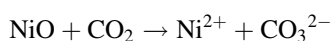
Cobalt substituted lithium–nickel oxides were synthesized by a solid-state reaction procedure using lithium nitrate, nickel hydroxide and cobalt oxalate precursor and were characterized as cathodes for molten carbonate fuel cell (MCFC).  $\text{LiNi}_{0.8}\text{Co}_{0.2}\text{O}_2$  cathodes were prepared using non-aqueous tape casting technique followed by sintering in air. The X-ray diffraction (XRD) analysis of sintered  $\text{LiNi}_{1-x}\text{Co}_x\text{O}_2$  indicated that lithium evaporation occurs during heating. The lithium loss decreases with an increase of the cobalt content in the mixed oxides. The stability studies showed that dissolution of nickel into the molten carbonate melt is smaller in the case of  $\text{LiNi}_{1-x}\text{Co}_x\text{O}_2$  cathodes compared to the dissolution values reported in the literature for state-of-the-art NiO. Pore volume analysis of the sintered electrode indicated a mean pore size of 3  $\mu\text{m}$  and a porosity of 40%. A current density of 160  $\text{mA}/\text{cm}^2$  was observed when  $\text{LiNi}_{0.8}\text{Co}_{0.2}\text{O}_2$  cathodes were polarized at 140 mV. The electrochemical impedance spectroscopy (EIS) studies done on  $\text{LiNi}_{0.8}\text{Co}_{0.2}\text{O}_2$  cathodes under different gas conditions indicated that the rate of the cathodic discharge reaction depends on the  $\text{O}_2$  and  $\text{CO}_2$  partial pressures.

© 2002 Published by Elsevier Science B.V.

*Keywords:* Cobalt substituted nickel oxide; Molten carbonate; Fuel cell; Dissolution

## 1. Introduction

Molten carbonate fuel cell (MCFC) technology is expected to be one of the most promising power generation systems for the coming century owing to its high efficiency and flexibility to a variety of fuels. These are high temperature fuel cells operating at a temperature of 650 °C, and have been under intensive development for the last few decades as a second-generation fuel cell [1,2]. Significant advances have been made in addressing design issues resulting in the development of prototype MCFC power generators. However, several problems remain before commercialization of MCFCs can be realized. The primary challenge remains in the proper selection of materials for the cathode and the current collector. In situ lithiated nickel oxide is in common use as a cathode material in the state-of-the-art MCFC [3]. Nickel oxide has a small degree of solubility in the molten carbonate eutectic melt used as an electrolyte in the MCFC [4] and does not satisfy long-term stability criteria [5]. Nickel oxide reacts with  $\text{CO}_2$  present in the electrolyte according to an acidic dissolution mechanism:



The dissolved nickel remains in equilibrium with the NiO cathode. Simultaneously, dissolved nickel ions diffuse from the cathode toward the anode under a concentration gradient. The dissolved nickel ions precipitate in the sections of matrix, where it encounters a reducing atmosphere due to the anode gas. The continuous diffusion of  $\text{Ni}^{2+}$  cation fuels more dissolution of nickel from the cathode [6,7]. Continued deposition of Ni in the anode region eventually leads to a short circuit between the anode and cathode. The cathode dissolution also results in loss of active material and a decrease of the active surface area available for the oxygen reduction reaction (cathodic reaction) leading to degradation in fuel cell performance.

Several materials like  $\text{LiFeO}_2$  and  $\text{LiCoO}_2$  were studied as replacement materials for NiO cathodes [8–10]. However, the exchange current density for the oxygen reduction reaction on  $\text{LiFeO}_2$  is about two orders of magnitude lower than that on NiO. Thus, the slow kinetics of the oxygen reduction limits further improvement of cathodes based on this material.  $\text{LiCoO}_2$  is more stable than NiO in alkaline environment [8]. However,  $\text{LiCoO}_2$  is less electronically conductive and is more expensive than NiO. Stoichiometric lithium–nickel oxides have good electronic conductivity when compared to other ceramic oxides like  $\text{LiFeO}_2$  and  $\text{LiCoO}_2$ . However, a significant lithium loss occurs on heating these lithiated nickel oxides. Due to this loss,

\* Corresponding author. Tel.: +1-803-777-7314; fax: +1-803-777-8265.  
E-mail address: popov@engr.sc.edu (B.N. Popov).

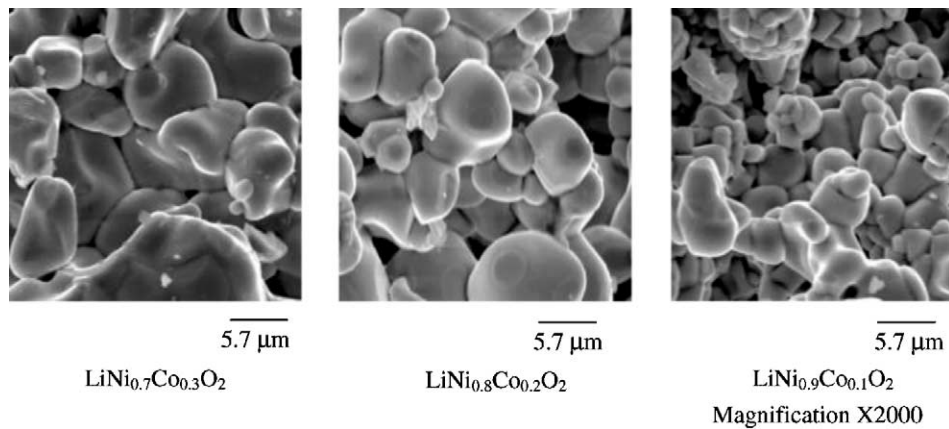


Fig. 1. The SEM of synthesized  $\text{LiNi}_{1-x}\text{Co}_x\text{O}_2$  with different amounts of cobalt doping ( $x = 0.1, 0.2$  and  $0.3$ ); magnification  $2000\times$ .

cathode conductivity will decrease causing poor cell performance. In this work, we have attempted to dope  $\text{LiNiO}_2$  with different amounts of cobalt using a solid-state route and tested  $\text{LiNi}_x\text{Co}_{1-x}\text{O}_2$  as cathodes in MFCs. Perez et. al. prepared  $\text{Li}_{1-x}(\text{Ni}_y\text{Co}_{1-y})_{1+x}\text{O}_2$  powders by powder metallurgy and sol-gel techniques for MFCs [12]. The objective of this study is to evaluate the performance of  $\text{LiNi}_x\text{Co}_{1-x}\text{O}_2$  as a cathode material in MFCs. A variety of electrochemical and physical characterization techniques have been used to study the performance of these mixed oxides.

## 2. Experimental

### 2.1. Material synthesis

Cobalt doped lithium–nickel oxides were prepared using a solid-state synthesis procedure. Stoichiometric amounts of lithium nitrate ( $\text{LiNO}_3$ ), nickel hydroxide [ $\text{Ni}(\text{OH})_2$ ] and cobalt oxalate ( $\text{CoC}_2\text{O}_4 \cdot 2\text{H}_2\text{O}$ ) obtained from the Aldrich were used as the starting precursors for the solid-state

synthesis. The compounds were mixed thoroughly and were heated in the presence of helium (regular grade, the National Welders). The temperature was initially kept at  $250^\circ\text{C}$  for about 5 h. This followed by heating at  $630^\circ\text{C}$  for 2 days. In both the cases, the temperature was increased at  $1^\circ\text{C}/\text{min}$ . After the helium treatment, the samples were heated in an oxygen atmosphere at  $800^\circ\text{C}$  for 20 h. Following this, the samples were finally heated in an autoclave at 500 psi  $\text{O}_2$  pressure at  $700^\circ\text{C}$  for 20 h. Fig. 1 shows the scanning electron micrographs (SEM) of synthesized  $\text{LiNi}_x\text{Co}_{1-x}\text{O}_2$ . As shown in Fig. 1,  $\text{LiNi}_{1-x}\text{Co}_x\text{O}_2$  particle size increases (from 5.7 to  $7.0\ \mu\text{m}$ ) with the increase of cobalt content in the solid solution.

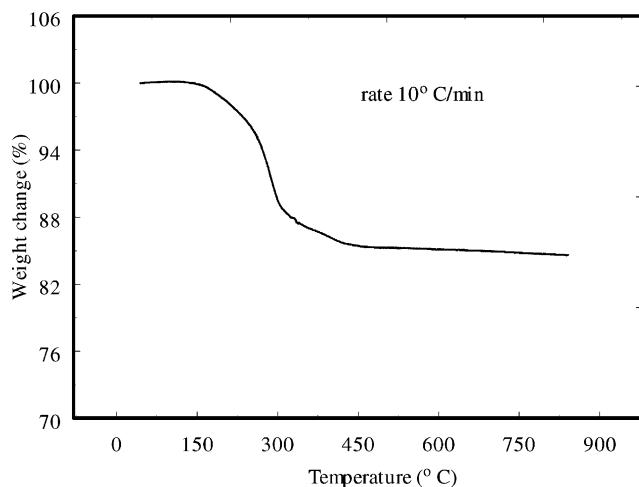


Fig. 2. The TGA of  $\text{LiNi}_{0.8}\text{Co}_{0.2}\text{O}_2$  tape obtained by non-aqueous tape casting.

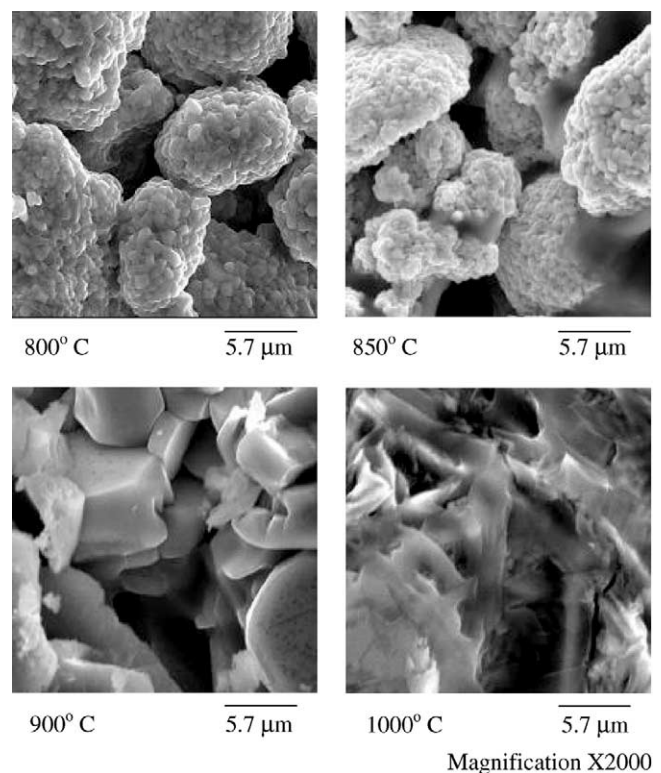


Fig. 3. The SEM pictures of  $\text{LiNi}_{0.8}\text{Co}_{0.2}\text{O}_2$  electrodes obtained after tape casting and sintering; magnification  $2000\times$ .

## 2.2. Tape casting

Porous  $\text{LiNi}_x\text{Co}_{1-x}\text{O}_2$  cathodes were made by a tape casting and sintering process.  $\text{LiNi}_x\text{Co}_{1-x}\text{O}_2$  particles (synthesized by solid-state reaction) were ground and sieved to obtain uniform particles of size 3–5  $\mu\text{m}$ . The tape casting slurry was prepared by ball milling  $\text{LiNi}_{1-x}\text{Co}_x\text{O}_2$  powder in xylene with a suitable binder (polyvinyl butyral (PVB)) and plasticizer (benzyl butyl phthalate and polyethylene glycol 50–50 vol.% mixture). The ball milling was done in two steps. In the first step, 50 g of  $\text{LiNi}_{1-x}\text{Co}_x\text{O}_2$  were added to 0.5 g of dispersant (GTO). The ingredients were mixed thoroughly with 32 ml of xylene and the slurry was ball milled for 6 h in order to break weak agglomerates. Next, 6 g of PVB and 4 ml of plasticizer mixture was added to the above suspension and the resulting slurry was ball milled for an additional 6 h. The slurry was then cast using a doctor blade assembly over a glass plate. The cast tapes were allowed to dry for 48 h. The cast plate  $\text{LiNi}_{1-x}\text{Co}_x\text{O}_2$  tape is then stripped off gently from the glass plate and stored.

## 2.3. Sintering

Sintering temperature of the tape cast electrodes influences the cathode pore structure and thereby affects its electrochemical performance. Thermo gravimetric analysis (TGA) was done to determine the optimum heat treatment schedule for sintering. A typical TGA curve for green  $\text{LiNi}_x\text{Co}_{1-x}\text{O}_2$  tape is as shown in Fig. 2. The cast  $\text{LiNi}_{1-x}\text{Co}_x\text{O}_2$  tape was pre-heated at 150 °C for 12 h in order to remove all the solvent in the tape. TGA analysis was done by heating the sample from 100 to 650 °C at a rate of 10 °C/min. A steep reduction in weight (12 wt.%) was seen on heating the sample between 200 and 400 °C due to the removal of the binder and plasticizer. The removal of all volatile and decomposable organic matter was completed below 400 °C. The total weight loss varied between 13 to 15 wt.% depending upon the binder and plasticizer contents of the green tapes. Fig. 3 shows the SEM of  $\text{LiNi}_{0.8}\text{Co}_{0.2}\text{O}_2$  tapes sintered at 800, 850 and 900 °C. Tapes sintered at 800 °C showed better pore structure. Based on the above

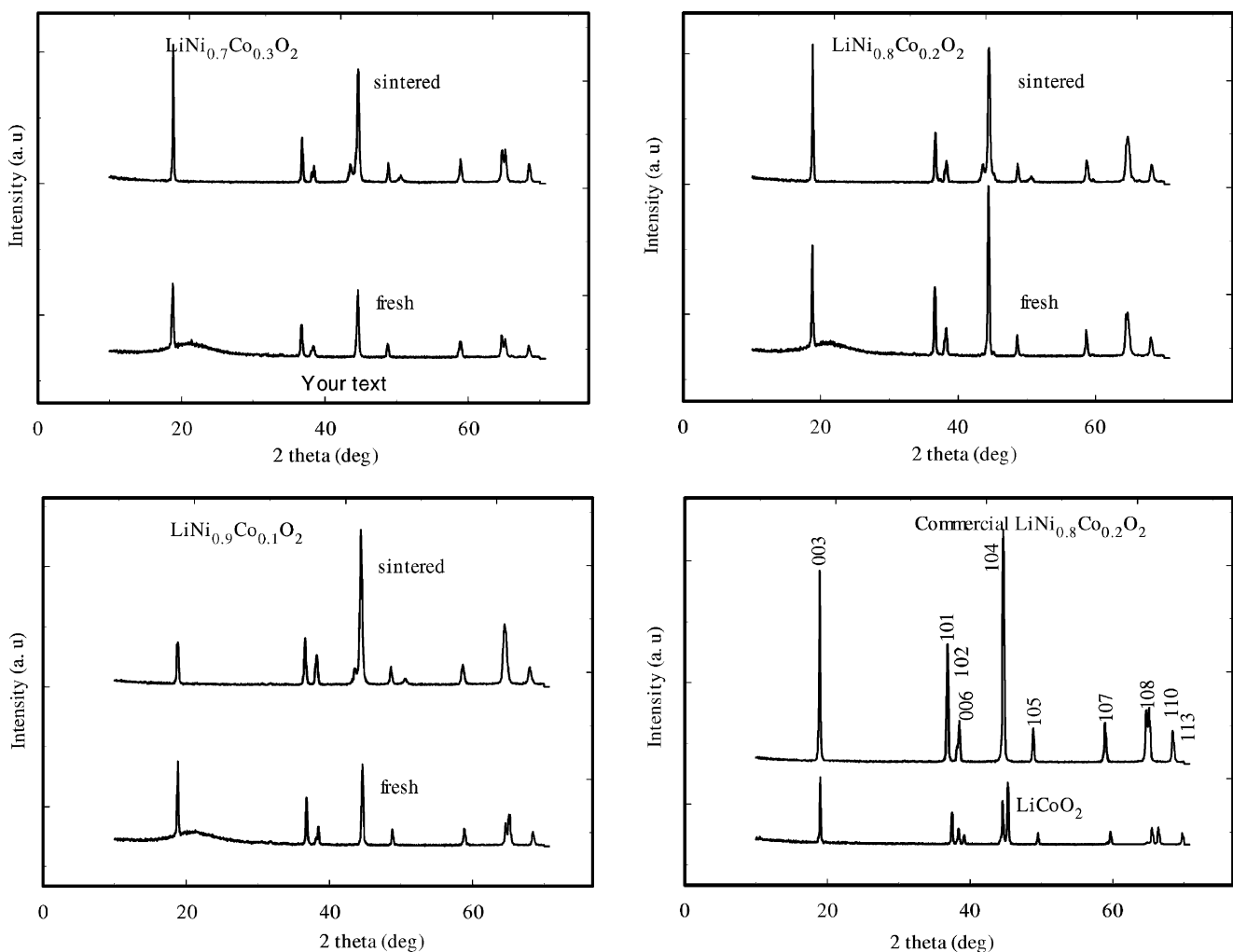


Fig. 4. The XRD patterns of pristine  $\text{LiCoO}_2$  and  $\text{LiNi}_{1-x}\text{Co}_x\text{O}_2$  solid solutions obtained by solid-state reaction procedure from lithium nitrate, nickel hydroxide and cobalt oxalate precursors. The XRD pattern of commercial  $\text{LiNi}_{0.8}\text{Co}_{0.2}\text{O}_2$  is shown for comparison.

TGA and SEM analysis, the following heating sequence was used—for sintering the electrodes: (i) green tapes which were cut and to specific areas ( $10\text{ cm} \times 10\text{ cm}$ ) and were initially heated from room temperature to  $150\text{ }^\circ\text{C}$  at a rate of  $1\text{ }^\circ\text{C}/\text{min}$  in air; (ii) in the second step, the temperature was held at  $150\text{ }^\circ\text{C}$  for 10 h; (iii) next, the temperature was raised to  $400\text{ }^\circ\text{C}$  at a rate of  $1\text{ }^\circ\text{C}/\text{min}$  in air; (iv) the temperature was held at  $400\text{ }^\circ\text{C}$  for 3 h; (v) the temperature was raised to  $800\text{ }^\circ\text{C}$  at  $1\text{ }^\circ\text{C}/\text{min}$  in air; (vi) the temperature was held at  $800\text{ }^\circ\text{C}$  for 1 h; and (vii) in the last step, the sample was cooled to room temperature using a cooling rate of  $1\text{ }^\circ\text{C}/\text{min}$ .

#### 2.4. Pot cell studies

In order to determine the solubility of  $\text{LiNi}_x\text{Co}_{1-x}\text{O}_2$ , pot tests were carried out under cathode gas conditions. Pellet electrodes of 1 cm diameter were made by hot pressing the  $\text{LiNi}_x\text{Co}_{1-x}\text{O}_2$  powders obtained using solid-state reaction. They were weighed and carefully dropped inside an alumina crucible containing 100 g of molten carbonate ( $\text{Li}_2\text{CO}_3/\text{K}_2\text{CO}_3 = 62/38$ ) at  $650\text{ }^\circ\text{C}$ . Cathode gas (30%  $\text{CO}_2/70\%$  air) was bubbled through the carbonate melt using alumina tubes. About 0.5 g of molten carbonate was taken from the

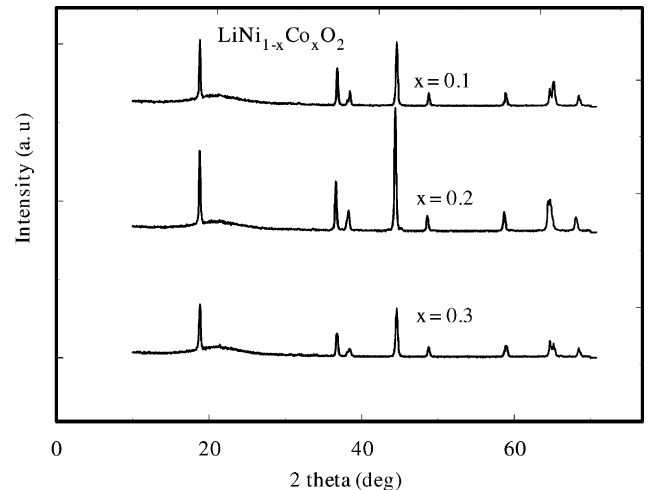


Fig. 5. The XRD patterns of  $\text{LiNi}_{1-x}\text{Co}_x\text{O}_2$  mixed oxides after sintering in air at  $800\text{ }^\circ\text{C}$  for 24 h.

melt approximately every 6 h up to 200 h using an alumina rod. The molten carbonate sample was dissolved in 10% dilute acetic acid. Atomic absorption (AA) spectroscopy was used to analyze the concentration of dissolved nickel.

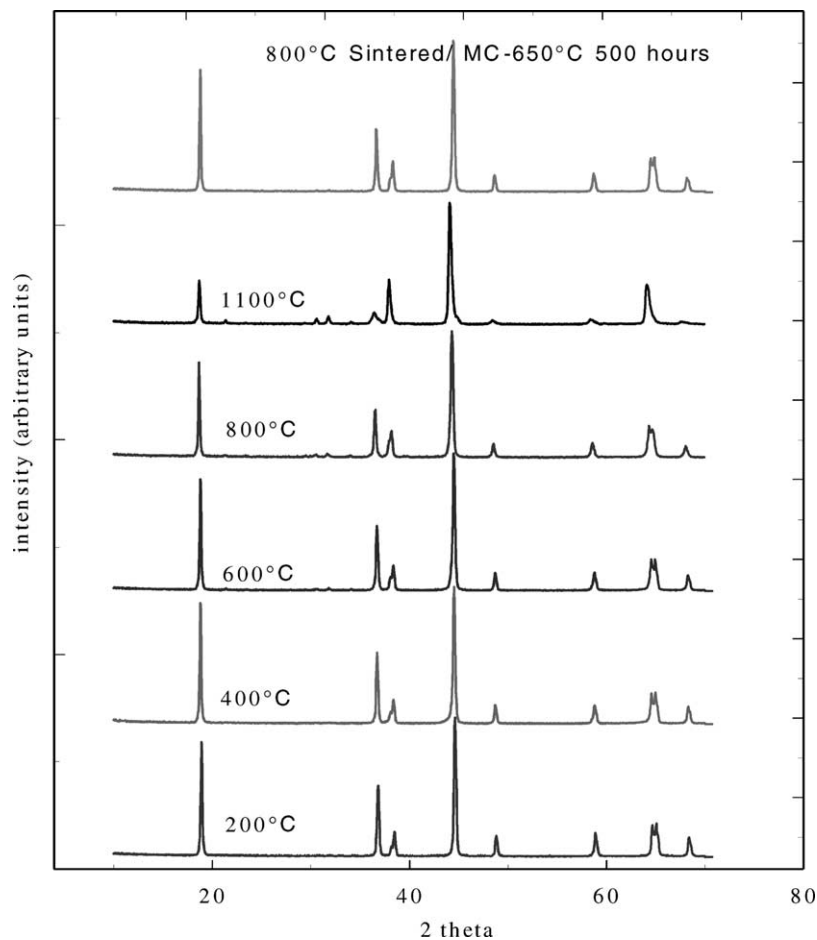


Fig. 6. The XRD patterns of  $\text{LiNi}_{0.8}\text{Co}_{0.2}\text{O}_2$  mixed oxides after sintering at different temperatures in air for 24 h.  $\text{LiNi}_{0.8}\text{Co}_{0.2}\text{O}_2$  sintered in molten carbonate eutectic at  $650\text{ }^\circ\text{C}$  for 500 h is shown for comparison.

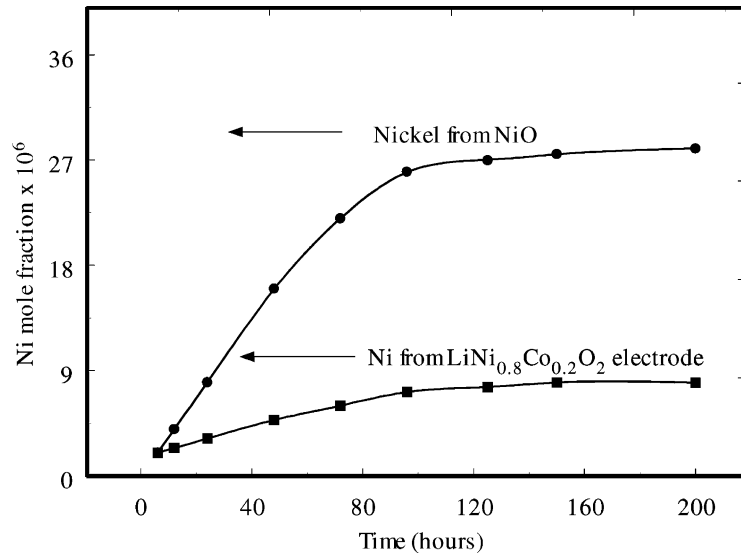


Fig. 7. The AA spectroscopy analysis of dissolved nickel in molten carbonate melt coming from  $\text{LiNi}_{0.8}\text{Co}_{0.2}\text{O}_2$  electrodes during immersion tests.

### 2.5. Electrochemical and material characterization

Half-cell performance studies were done in a  $3\text{ cm}^2$ -lab cell [21].  $\text{LiNi}_{0.8}\text{Co}_{0.2}\text{O}_2$  was used as the working and counter electrodes.  $(\text{Li}_{0.62}\text{K}_{0.38})_2\text{CO}_3$  eutectic embedded in a  $\text{LiAlO}_2$  matrix was used as the electrolyte. Polarization studies were done using an oxidant gas composition of 70% air and 30%  $\text{CO}_2$ . Two oxygen reference electrodes ( $\text{Au}/\text{CO}_2/\text{O}_2$ ) connected to the electrolyte tile with a salt bridge (50%  $(\text{Li}_{0.62}\text{K}_{0.38})_2\text{CO}_3$  + 50%  $\text{LiAlO}_2$ ) were used to monitor the polarization of the cathode. Electrochemical impedance spectroscopic (EIS) studies were performed using a Model 1255 Schlumberger frequency analyzer. The electrode was stable during the experiments and its open circuit potential changed  $<1\text{ mV}$ . The impedance data generally covered a frequency range of 1 mHz to 100 kHz. A sinusoidal ac voltage signal varying by  $\pm 5\text{ mV}$  was applied in all cases. The X-ray diffraction (XRD) was used to study the crystal structure of the samples. Mercury porosimeter was used to characterize the pore-volume distribution of the sintered cathodes.

## 3. Results and discussions

### 3.1. X-ray diffraction studies

Fig. 4 shows powder XRD patterns of pristine  $\text{LiCoO}_2$  and  $\text{LiNi}_{1-x}\text{Co}_x\text{O}_2$  solid solutions. These patterns reveal that all these materials are single phase with the  $\alpha\text{-NaFeO}_2$  structure, space group  $R3m$ . The transition metal ions are in turn surrounded by six oxygen atoms. Infinite layers of  $\text{Ni}_{1-x}\text{Co}_x\text{O}_2$  were formed through edge sharing of the  $(\text{Ni}_{1-x}\text{Co}_x\text{O}_6)$  octahedra, with the intercalating lithium ions located between the layers. All of the diffraction lines

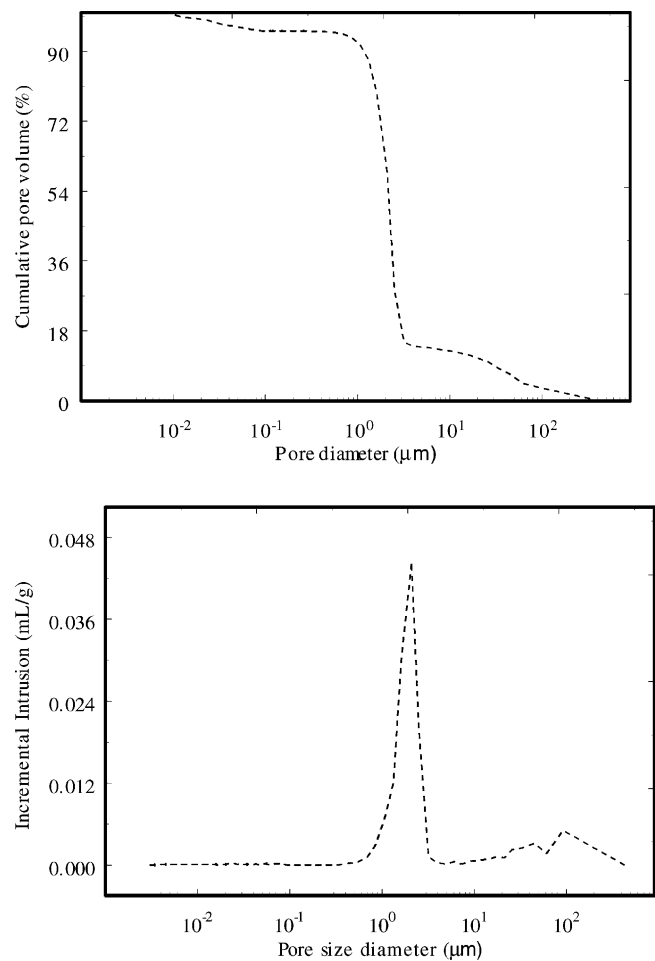


Fig. 8. Pore volume distribution obtained on  $\text{LiNi}_{0.8}\text{Co}_{0.2}\text{O}_2$  electrodes by mercury intrusion method.

of  $\text{LiNi}_{1-x}\text{Co}_x\text{O}_2$  can be indexed with a hexagonal lattice. Analytical results were obtained from the XRD data using the lines (0, 0, 3) and (1, 0, 4). As the  $\text{Ni}^{3+}$  ions at the 3(a) sites of the  $\text{LiNiO}_2$  lattice are partially replaced by  $\text{Co}^{3+}$  ions, the unit cell dimensions,  $a$  and  $c$ , in a hexagonal setting become smaller. The lattice constants were  $a = 2.876 \text{ \AA}$  and  $c = 14.183 \text{ \AA}$  for  $\text{LiNi}_{0.9}\text{Co}_{0.1}\text{O}_2$ ;  $a = 2.871 \text{ \AA}$  and  $c = 14.176 \text{ \AA}$  for  $\text{LiNi}_{0.8}\text{Co}_{0.2}\text{O}_2$ ;  $a = 2.865 \text{ \AA}$  and  $c = 14.170 \text{ \AA}$  for  $\text{LiNi}_{0.7}\text{Co}_{0.3}\text{O}_2$  and  $a = 2.816 \text{ \AA}$  and  $c = 14.046 \text{ \AA}$  for  $\text{LiCoO}_2$ . This decrease in lattice constants is due to the difference in size between trivalent cobalt and trivalent nickel ions ( $r_{\text{Ni}^{3+}} = 0.56 \text{ \AA}$ ,  $r_{\text{Co}^{3+}} = 0.53 \text{ \AA}$ ) [11]. These results strongly suggest that  $\text{LiNi}_x\text{Co}_{1-x}\text{O}_2$  is in a homogenous phase, i.e.  $\text{Ni}^{3+}$  and  $\text{Co}^{3+}$  are homogeneously located at the octahedral 3(a) sites in a cubic phased oxygen array.

Fig. 5 compares the XRD patterns of  $\text{LiNi}_x\text{Co}_{1-x}\text{O}_2$  sintered at  $800 \text{ }^\circ\text{C}$  for a period of 24 h in the presence of air. The XRD patterns indicate that the (0, 0, 3) line characteristic of the lithium content decrease for the case of  $\text{LiNi}_{0.9}\text{Co}_{0.1}\text{O}_2$ . As the cobalt content increases in the  $\text{LiNi}_{1-x}\text{Co}_x\text{O}_2$  ( $x = 0.1, 0.2$  and  $0.3$ ), the lithium evaporation on heating also decreases. Perez et al. [12] carried out a similar experiment, wherein they treated different  $\text{Li}(\text{NiCo})$  mixed oxides in molten carbonate at  $650 \text{ }^\circ\text{C}$  under air and observed a decrease in lithium content in the oxides. Fig. 6 shows the XRD patterns of  $\text{LiNi}_{0.8}\text{Co}_{0.2}\text{O}_2$  heat treated at different temperatures for a period of 24 h. It is seen that the  $\text{LiNi}_{0.8}\text{Co}_{0.2}\text{O}_2$  is quite stable up to sintering temperatures of  $800 \text{ }^\circ\text{C}$  in terms of lithium content. Heating  $\text{LiNi}_{0.8}\text{Co}_{0.2}\text{O}_2$  to  $1100 \text{ }^\circ\text{C}$  leads to a lot of lithium loss, which is seen, from the different XRD pattern obtained. Also, the XRD pattern obtained from  $\text{LiNi}_{0.8}\text{Co}_{0.2}\text{O}_2$  samples heat treated in molten

carbonate for 500 h under air at  $650 \text{ }^\circ\text{C}$  shows no significant structural change when compared to the pristine oxide. These results show that  $\text{LiNi}_{1-x}\text{Co}_x\text{O}_2$  ( $x = 0.2, 0.3$ ) may exhibit the structural integrity needed of a MCFC cathode to sustain long-term operation.

### 3.2. Stability tests

The short-term stability of  $\text{LiNi}_{0.8}\text{Co}_{0.2}\text{O}_2$  in molten carbonate eutectic was determined using pot tests. AA was used to analyze the dissolved nickel in the melt. Fig. 7 shows the results from AA analysis of the amount of dissolved nickel in the carbonate melt as a function of time. The results indicate that cobalt doping increases the resistivity of the oxide to the molten carbonate environment. The amount of nickel cation in the carbonate melt increases with time and stabilizes after about 100 h. The dissolution rate obtained for  $\text{LiNi}_{0.8}\text{Co}_{0.2}\text{O}_2$  is about one-half of the dissolution of state-of-the-art nickel oxide reported in literature [13–17]. Based on these results and the XRD data, it was decided to carry out further studies on  $\text{LiNi}_{0.8}\text{Co}_{0.2}\text{O}_2$ . These compounds exhibit sufficient stability at operating temperatures and, also, the rate of dissolution of nickel is lower when compared to state-of-the-art cathodes.

### 3.3. Pore volume distribution

The electrode structure is one of the principal factors determining cell performance in MCFCs. The electrode reaction takes place mainly near the meniscus (three phase boundary), where mass transport resistance is least for gas diffusing through the liquid to the reaction surface. Alternatively an electrolyte film may cover the pore wall through

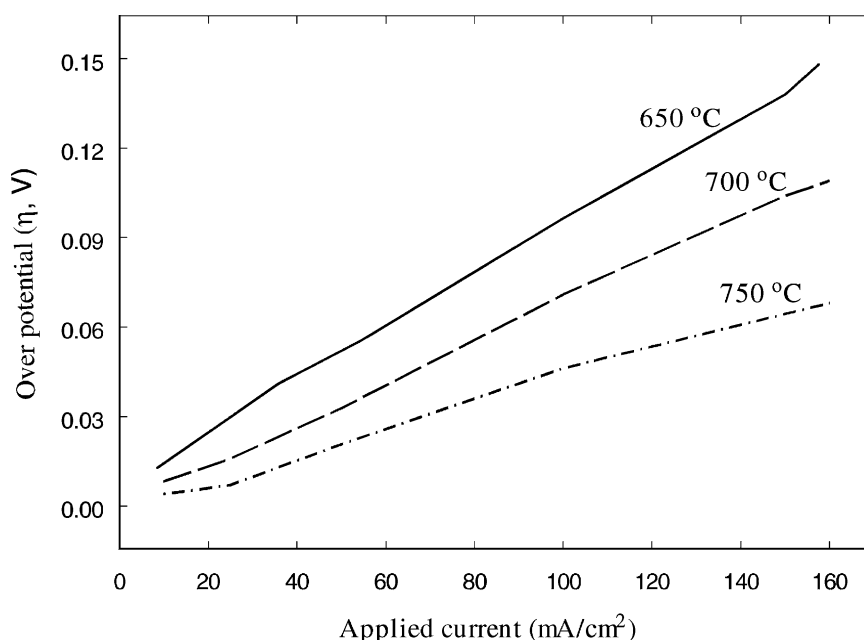


Fig. 9. Comparison of cathode polarization behavior at different temperatures for  $\text{LiNi}_{0.8}\text{Co}_{0.2}\text{O}_2$  cathodes.

which the gas diffuses to the electrode. Flooding of the electrode is usually deleterious to the performance of cathodes. Cathode porosity is adjusted in order to ensure proper electrolyte distribution. Small pores retain electrolyte by capillary pressure, while large pores are gas-filled, even though their walls may be fully or partly wetted by thin liquid films. Fig. 8 shows the pore volume distribution of sintered  $\text{LiNi}_{0.8}\text{Co}_{0.2}\text{O}_2$  cathodes. The pore size distribution shows three kinds of pores ranging from micropores of  $<1\ \mu\text{m}$  size to macropores of size  $>10\ \mu\text{m}$ . The majority of the pores lay in the intermediate class of particle size around  $2\sim 3\ \mu\text{m}$ . The porosity of the sintered  $\text{LiNi}_{0.8}\text{Co}_{0.2}\text{O}_2$  cathode was 38.50. This value is lower when compared to the porosity of in situ sintered state-of-the-art NiO cathode (porosity  $\sim 50\text{--}55\%$ ) [18]. This low porosity in the case of

$\text{LiNi}_{0.8}\text{Co}_{0.2}\text{O}_2$  cathodes can cause high polarization during testing. However, porosity can be enhanced by the addition of pore formed during tape casting and by careful optimization of sintering conditions.

#### 3.4. Polarization studies

Polarization studies were carried out in a three electrode  $3\ \text{cm}^2$ -lab scale cell containing  $\text{LiNi}_{0.8}\text{Co}_{0.2}\text{O}_2$  electrodes both as the working and counter electrodes. Gold (oxygen reduction) served as a reference electrode. The electrodes were separated by a  $\text{LiAlO}_2$  ceramic tile containing Li/K carbonate melt (62–38 mol%). The cell is connected to a gold/oxygen reference electrode through a salt bridge. The polarization characteristics  $\text{LiNi}_{0.8}\text{Co}_{0.2}\text{O}_2$  cathodes were

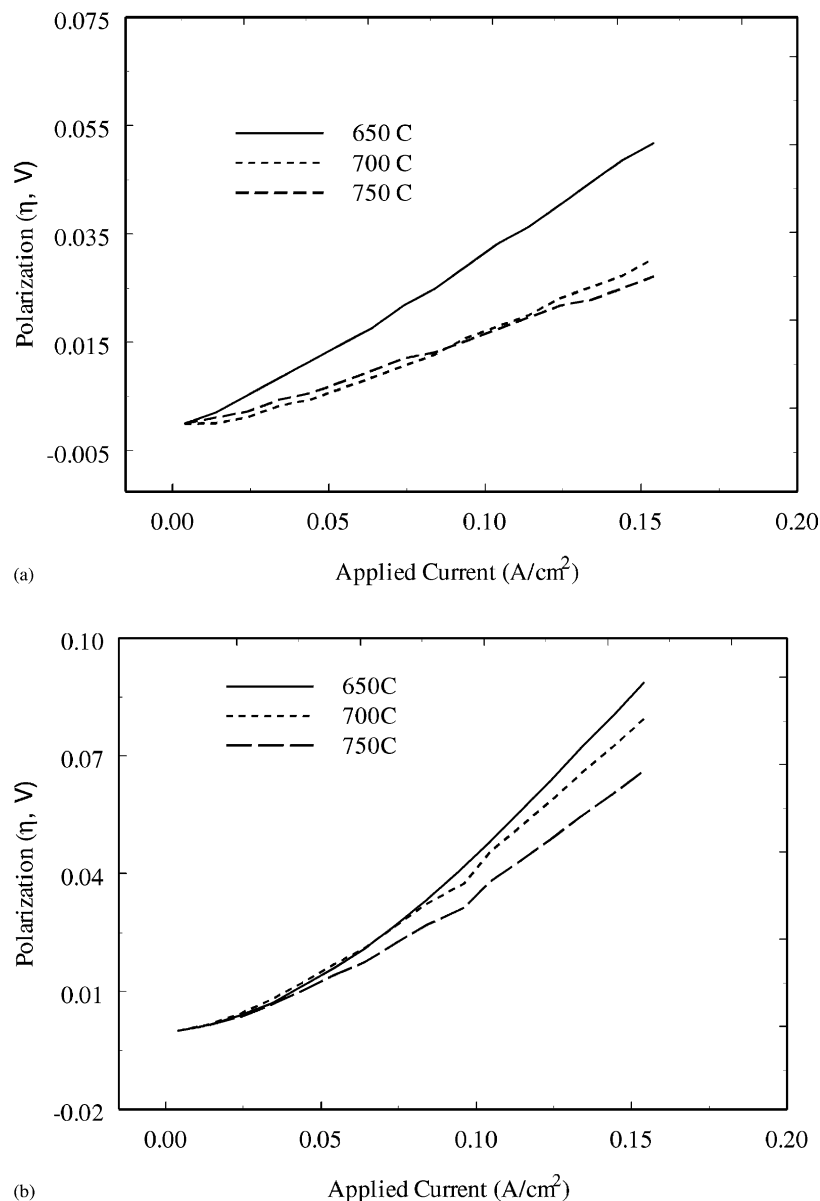


Fig. 10. Polarization behavior of: (a) Nickel and (b) cobalt encapsulated nickel electrodes at different operating temperatures.



obtained by varying the current load. Fig. 9 compares the cathode polarization during the galvanodynamic scan for the  $\text{LiNi}_{0.8}\text{Co}_{0.2}\text{O}_2$  electrode at different operating temperatures. The current was scanned at 1 mA/s and the curves have been corrected for  $IR$  loss based on  $R_W$  calculated from impedance measurements (not shown).

The  $i-\eta$  characteristics of  $\text{LiNi}_{0.8}\text{Co}_{0.2}\text{O}_2$  cathodes obtained at different temperatures are similar to each other. Increasing the temperature has a significant influence on the polarization in the case of  $\text{LiNi}_{0.8}\text{Co}_{0.2}\text{O}_2$ . The observed

over potentials,  $\eta$ , decrease with increasing the temperature indicating a decrease of both the polarization and diffusion over potentials with an increase of temperature. The voltage polarization at an applied current of  $160 \text{ mA/cm}^2$ , decreased from 140 mV at  $650^\circ\text{C}$  to 65 mV at  $750^\circ\text{C}$  as shown in Fig. 9. Similar results were observed in the literature in the case of NiO electrodes [19–21]. Our earlier study showed a voltage polarization of 55 mV for NiO and 95 mV for Co encapsulated nickel electrodes for an applied current of  $160 \text{ mA/cm}^2$ . Fig. 10 shows the effect of temperature on

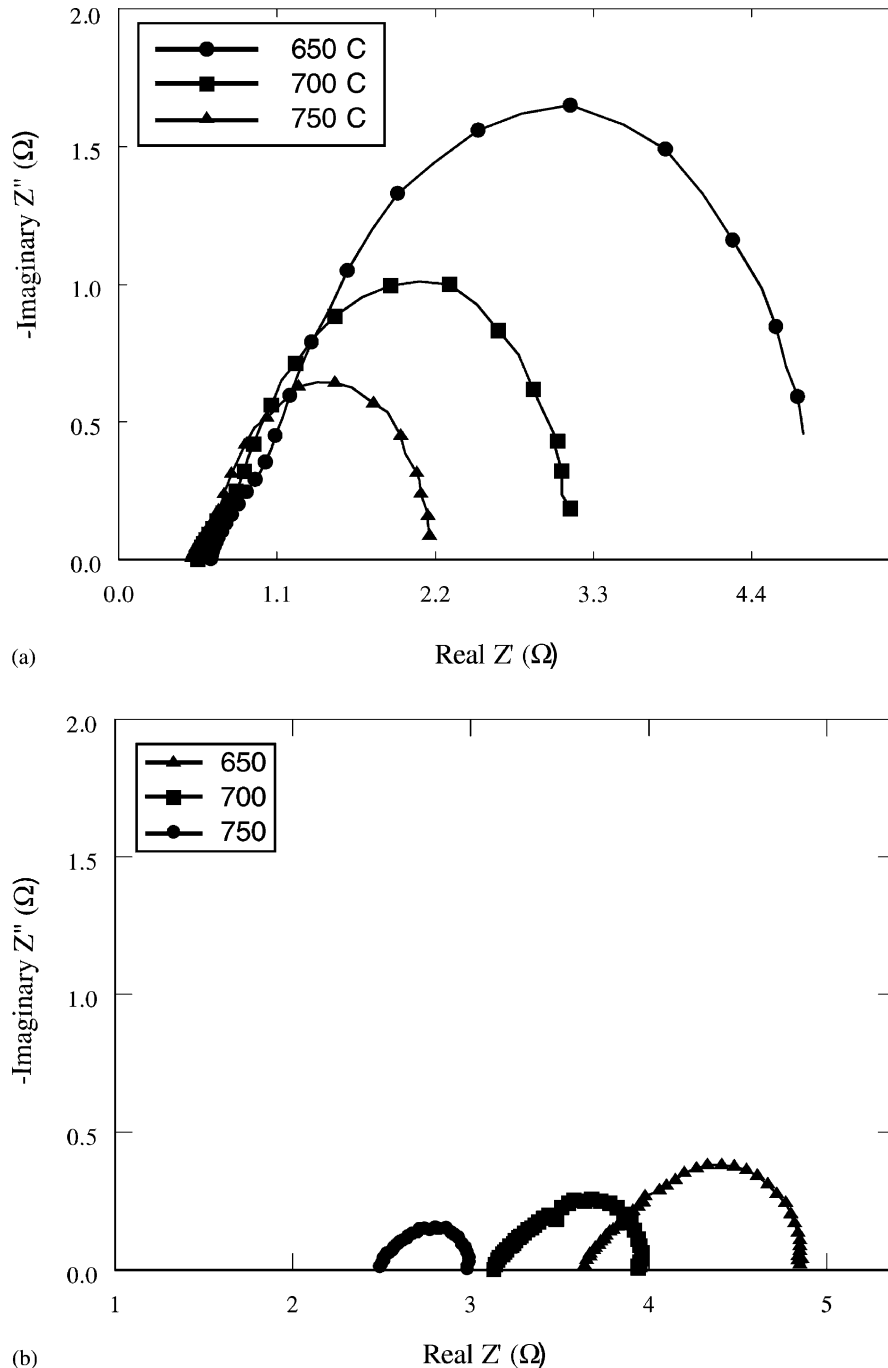


Fig. 11. Nyquist plots of: (a)  $\text{LiCoO}_2$  and (b) NiO at different operating temperatures in standard cathode gas atmosphere ( $\text{CO}_2:\text{O}_2$ , 66:33%).

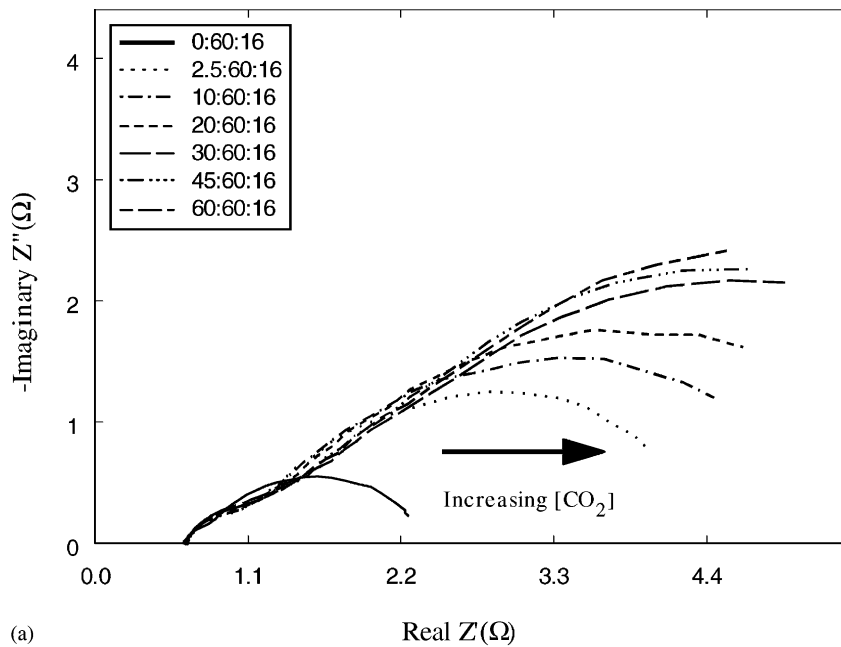


cathode polarization of NiO and Co encapsulated NiO. This difference in the performance of  $\text{LiNi}_{0.8}\text{Co}_{0.2}\text{O}_2$  and NiO cathodes can be attributed to the low porosity ( $\sim 45\%$ ) of the  $\text{LiNi}_{0.8}\text{Co}_{0.2}\text{O}_2$  cathodes.

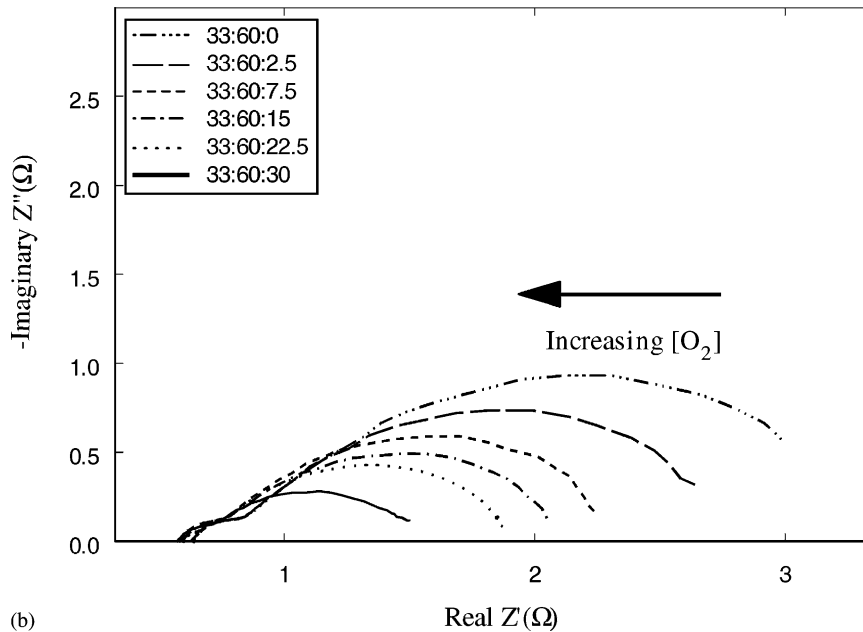
The performance of the  $\text{LiNi}_{0.8}\text{Co}_{0.2}\text{O}_2$  electrodes was evaluated from the exchange current density data obtained from  $i$ - $V$  plots under low current load ( $i \leq 10 \text{ mA/cm}^2$ ). The slope of the linear part of  $i$ - $V$  curve was used to calculate the apparent exchange density based on the expression  $i_0 = RT/nFR_{ct}$ , where  $R$  is the universal gas constant,  $T$

Table 1  
Exchange current density values obtained for different cathode materials at  $650^\circ\text{C}$  under normal cathode gas atmosphere ( $\text{CO}_2:\text{O}_2$ , 66:33%)

Material	Exchange current density ( $i_0$ ) (mA/cm <sup>2</sup> )
NiO <sup>21</sup>	31
Co encapsulated NiO <sup>21</sup>	16.1
$\text{LiNi}_{0.8}\text{Co}_{0.2}\text{O}_2$	26.1



(a)



(b)

Fig. 12. Nyquist plots of impedance response of  $\text{LiNi}_{0.8}\text{Co}_{0.2}\text{O}_2$  electrode as a function of  $\text{O}_2$  and  $\text{CO}_2$  partial pressures at  $650^\circ\text{C}$  (a and b),  $700^\circ\text{C}$  (c and d) and  $750^\circ\text{C}$  (e and f) (the numbers in parenthesis indicates the  $\text{CO}_2$ ,  $\text{N}_2$  and  $\text{O}_2$  concentrations in  $\text{cm}^3/\text{min}$ ).

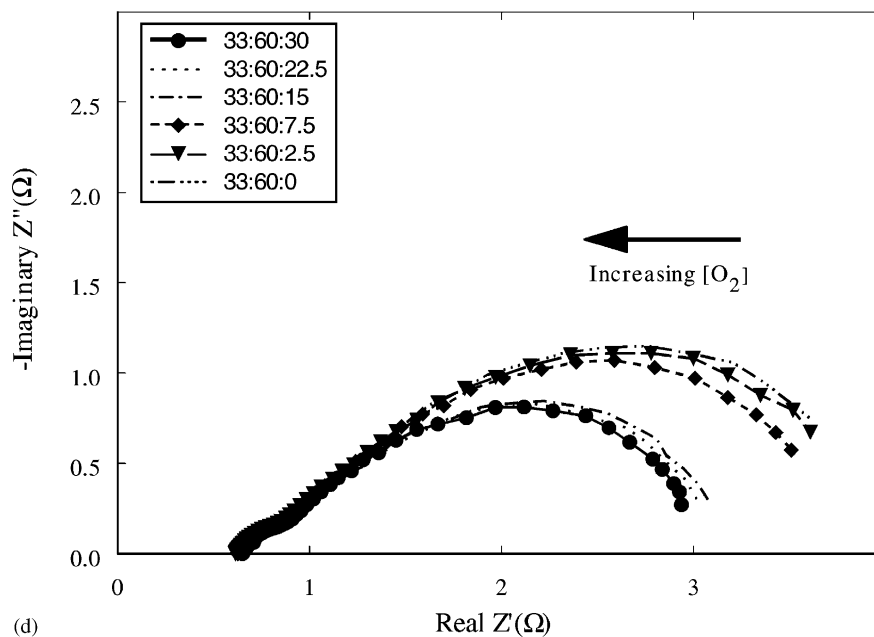
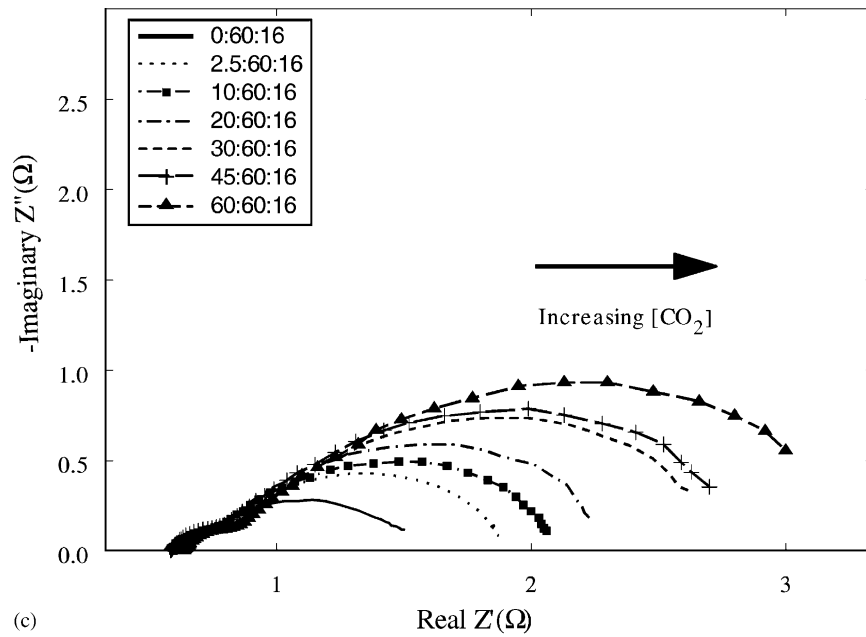


Fig. 12. (Continued).

the cell temperature,  $F$  Faraday's constant and  $R_{ct}$  is the slope of the  $i$ - $V$  response. The range of the values of exchange current density calculated for  $\text{LiNi}_{0.8}\text{Co}_{0.2}\text{O}_2$  cathodes varied from 25.1 to 26.1  $\text{mA}/\text{cm}^2$  during various stages of operation. The apparent exchange current density calculated using the same method for the case of NiO in one of our earlier studies varied between 29 and 31  $\text{mA}/\text{cm}^2$  [21]. The exchange current density for NiO, Co encapsulated nickel and  $\text{LiNi}_{0.8}\text{Co}_{0.2}\text{O}_2$  electrodes are as shown in Table 1. The low exchange current density observed could again be due to the lower porosity of  $\text{LiNi}_{0.8}\text{Co}_{0.2}\text{O}_2$  cathodes.

### 3.5. Electrochemical impedance spectroscopy studies

In order to understand the kinetics of oxygen reduction on  $\text{LiNi}_{0.8}\text{Co}_{0.2}\text{O}_2$ , impedance measurements were carried out at different gas compositions. The EIS analysis was carried out at open circuit on the  $\text{LiNi}_{0.8}\text{Co}_{0.2}\text{O}_2$  electrodes. Fig. 11 shows the impedance analysis of NiO and  $\text{LiCoO}_2$  electrodes at different temperatures at a particular gas composition. The impedance response at any given temperature is characterized by the presence of a high frequency loop and an extension at low frequencies. The high frequency plot has

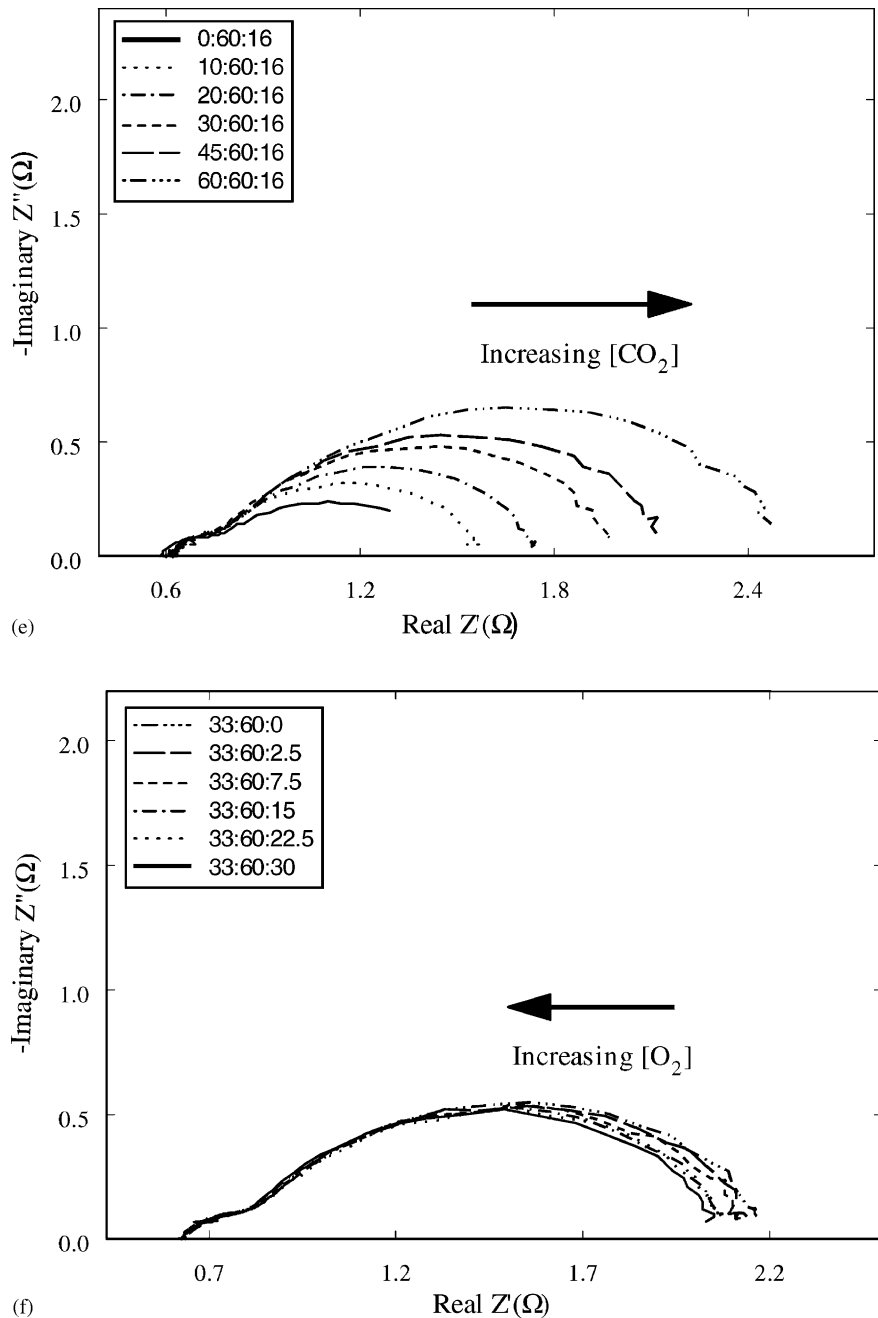


Fig. 12. (Continued).

been associated with the charge transfer processes and the low frequency loop with a slow process (mass transfer). The impedance response as shown in Fig. 12(a–f) is similar in appearance to the ones obtained by Yuh and Selman [19,20] under similar conditions for NiO cathodes. As shown in Fig. 12(a–f), the cell temperature has a marked effect on the ac impedance. On increasing the temperature, a drastic decrease of charge transfer resistance is seen, which is in agreement with the results obtained from polarization studies.

From Fig. 12(a–f), it can also be seen that the effect of partial pressure of O<sub>2</sub> and CO<sub>2</sub> are opposed to each other.

The magnitude of the impedance loop decreased on increasing the O<sub>2</sub> partial pressure. This clearly indicates a positive reaction order for oxygen and is similar to the response seen for NiO [20]. In the case of CO<sub>2</sub>, the impedance value increased with an increase in CO<sub>2</sub> partial pressures implying that the reaction order of CO<sub>2</sub> must be negative. Yuh and Selman [20] obtained similar results for NiO in terms of O<sub>2</sub> and CO<sub>2</sub> dependence on impedance responses. This shows that the oxygen reduction kinetics in LiNi<sub>0.8</sub>Co<sub>0.2</sub>O<sub>2</sub> follows a similar mechanism as in that of NiO. Hence, LiNi<sub>0.8</sub>Co<sub>0.2</sub>O<sub>2</sub> can be used as a cathode material for MCFC applications.

#### 4. Conclusions

$\text{LiNi}_{1-x}\text{Co}_x\text{O}_2$  was synthesized by solid-state reaction from lithium nitrate, nickel hydroxide and cobalt oxalate precursors. Lithium loss occurred during sintering of these mixed oxides but this loss gradually decreased with the increase in cobalt content.  $\text{LiNi}_{0.8}\text{Co}_{0.2}\text{O}_2$  showed lower rate of dissolution in molten carbonate under cathode gas conditions when compared to that of NiO. However, considering the economy of cobalt doping, and stability at higher temperatures,  $\text{LiNi}_{0.8}\text{Co}_{0.2}\text{O}_2$  was chosen for further characterization studies.  $\text{LiNi}_{0.8}\text{Co}_{0.2}\text{O}_2$  cathodes for MCFC were made by a tape casting and sintering process. The SEM analysis of  $\text{LiNi}_{0.8}\text{Co}_{0.2}\text{O}_2$  electrodes sintered at 800 °C showed good pore structure. Pore volume distribution studies done using mercury porosimetry showed lower porosity when compared to that of the state-of-the-art cathode. The  $i$ - $V$  characteristics of  $\text{LiNi}_{0.8}\text{Co}_{0.2}\text{O}_2$  were good with a current drain of 160 mA/cm<sup>2</sup> for a voltage polarization ( $IR$  free) of 140 mV. Impedance spectroscopic studies done on  $\text{LiNi}_{0.8}\text{Co}_{0.2}\text{O}_2$  under different gas conditions indicated that the oxygen reduction reaction mechanism follows a positive order for O<sub>2</sub> concentration and a negative reduction order for CO<sub>2</sub>. This suggests that the oxygen reduction mechanism is qualitatively similar to that of the state-of-the-art cathodes listed in the literature. Finally,  $\text{LiNi}_{0.8}\text{Co}_{0.2}\text{O}_2$  can be regarded as an alternative material to the conventional nickel oxide cathodes in MCFCs.

#### Acknowledgements

Financial support by the National Energy Technology Laboratory (NETL), which is supported by the US Department of Energy (DOE), is gratefully acknowledged.

#### References

- [1] A.J. Appleby, F.R. Foulkes, Fuel Cells—Hand Book, Van Nostrand Reinhold, New York, 1989.
- [2] K. Joon, J. Power Sources 71 (1998) 12.
- [3] J.R. Selman, in: S.S. Penner (Ed.), Assessment of Research Needs for Advanced Fuel Cells by The DOE Advanced Fuel Cell Working Group (AFCWG), Pergamon Press, New York, 1984.
- [4] T.G. Benamin, E.L. Camara, L.G. Marianowski, Handbook of Fuel Cell Performance, Contract no. EC-77C-03-1545, Chicago, IL, 1980.
- [5] L. Christner, L. Paetsch, P. Patel, M. Farooque, Scale-up of internal reforming molten carbonate fuel cells, in: Proceedings of the Fuel Cell Seminar, Long Beach, CA, 1988, p. 403.
- [6] Development of Molten Carbonate Fuel Cell Power Plant, Final Report DOE/ET/17019-20, General Electric Company, March 1985.
- [7] R.D. Pierce, J.L. Smith, R.B. Poeppel, in: J. R. Selman, T.D. Claar (Eds.), Molten Carbonate Fuel Cell Technology, PV 84-13, Proceedings of the Electrochemical Society Series, Pennington, NJ, 1984, p. 147.
- [8] L. Plomp, E.F. Sitters, C. Vessies, F.C. Eckes, J. Electrochem. Soc. 138 (2) (1991) 629.
- [9] L. Giorgi, M. Carewska, S. Scaccia, E. Simonetti, F. Zarzana, Denki Kagaku 64 (6) (1996) 482.
- [10] C. Lagergren, A. Lundblad, B. Bergman, J. Electrochem. Soc. 141 (11) (1994) 2959.
- [11] R.D. Shannon, G.T. Prewitt, Acta Crystallogr., Sect. B 25 (1969) 925.
- [12] F.J. Perez, D. Duday, M.P. Hierro, C. Gomez, M. Romero, M.T. Casais, J.A. Alonso, M.J. Martinez, L. Daza, J. Power Sources 86 (2000) 309–315.
- [13] K. Tanimoto, Y. Miyazaki, M. Yanagida, S. Tanase, T. Kojima, N. Ohtori, H. Okuyama, T. Kodama, Denki Kagaku 59 (7) (1991) 619.
- [14] K. Ota, S. Mitsushima, S. Katao, S. Asano, H. Yoshitake, N. Kamiya, J. Electrochem. Soc. 139 (3) (1992) 667.
- [15] X. Zhang, P. Capobianco, A. Torazza, B. Passalacqua, Electrochemistry 67(6) (1999).
- [16] J.B.J. Veldhuis, F.C. Eckes, L. Plomp, J. Electrochem. Soc. 139 (1) (1992) L6.
- [17] K. Ota, Y. Takeishi, S. Shibata, H. Yoshitake, N. Kamiya, J. Electrochem. Soc. 142 (10) (1995) 3322.
- [18] S. S. Penner (Ed.), Assessment of Research Needs for Advanced Fuel Cells by DOE advanced Fuel Cell Working Group, Pergamon Press, New York, 1985.
- [19] C.Y. Yuh, J.R. Selman, J. Electrochem. Soc. 138 (12) (1991) 3642.
- [20] C.Y. Yuh, J.R. Selman, J. Electrochem. Soc. 138 (12) (1991) 3649.
- [21] A. Durairajan, H. Colon, B. Haran, R.E. White, B.N. Popov, J. Power Sources 104 (2) (2002) 157–168.